Transactions, SMiRT-24
BEXCO, Busan, Korea - August 20-25, 2017
Division VI

A Discussion of Cracked Concrete Properties for Accidental Thermal Analysis

Adeola Adediran[1], Partha Ghosal[2]

[1] CSA/SM Functional Engineering Manager, Savannah River Remediation LLC, Contractor to Department of Energy, South Carolina. USA
[2] Senior Program Manager, Tennessee Valley Authority, Tennessee. USA.

ABSTRACT

As members of ACI 349 code committee, we have struggled with the guidance that is given in ACI 349.1R (2007) that calculates cracked moment of inertia as 50% of the gross moment of inertia for all thermal analysis. This guidance of 50% has been translated into $0.5E_cI_g$ in Elastic Finite Element Analyses (FEAs). Recently ACI 349.1R in development is proposing that the cracked properties for thermal analysis use the cracked modulus of elasticity stated in ASCE 43. This provision, provided as conservative guidance only, traditionally has had no limits to its applicability either for the type of structural components (i.e. columns, beam, walls or slabs) or to the temperature range (i.e. operating thermal temperature limits or accidental thermal temperature limit). Routinely cracked concrete properties are used to reduce the thermal moments that a structural component is checked for because of the self-relieving nature of such stresses when cracking occurs. This paper presents a numerical study of cracked properties that accounts for thermal cracking of frames and compares the results to the recommendations in ASCE 43 and to the $0.5E_cI_g$ conservative guidance in ACI 349.1R. The results of this parametric study can be extended to walls and slabs as well.

OVERVIEW OF ANALYTICAL PROCEDURE

This parametric study is benchmarked to the example problem in ACI 349.1R. This example problem is a frame given in Figure 1. As recommended by ACI 349.1R the frame is analysed for the mechanical loads first assuming un-cracked geometric properties. A linear elastic analysis is deemed bounding for accidental thermal load analysis and is recommended by ACI 349 to be used in design. Therefore this was used in this parametric study. To simplify the analysis, concrete tensile strength, tension stiffening, strain hardening and non-linear thermal gradients are ignored. The analytical process used for the parametric study is given in Figure 2 and discussed in subsequent subsections.

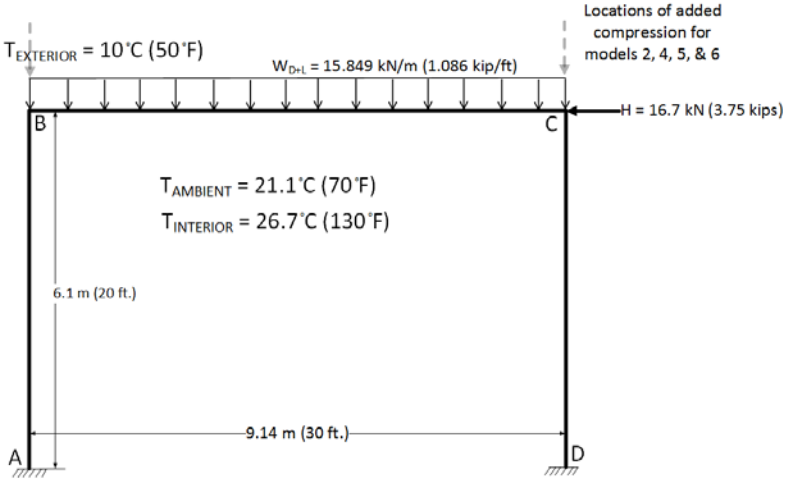

Figure 1 - Frame under Mechanical and Thermal Loads for the Benchmark Example

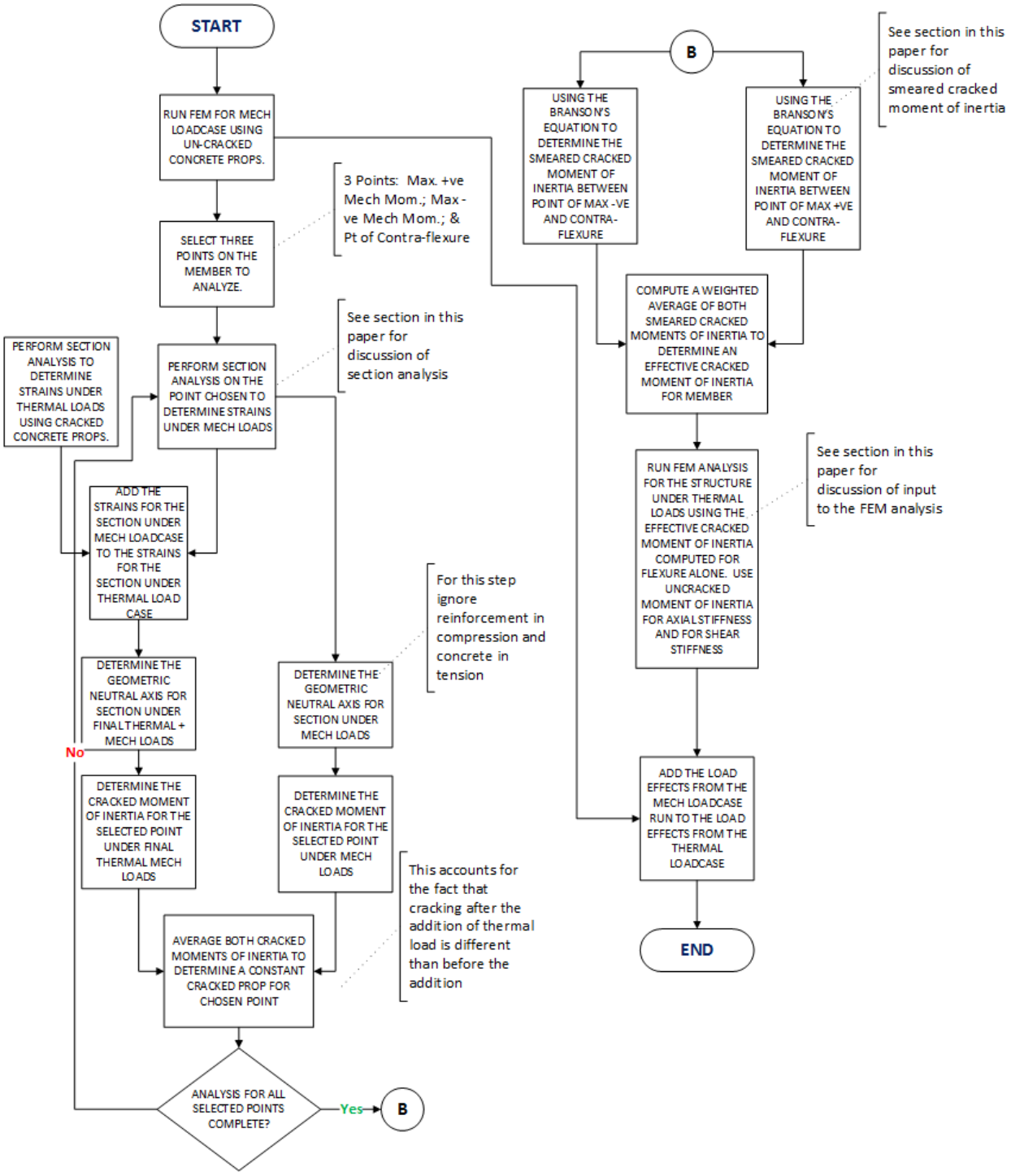

Figure 2 - Analytical Process Used

Concrete Section

The frame is given in ACI 349.1R to have the same cross section in the beam as in the column. This cross section is given in Figure 3. The properties given for this cross section are as follows:

Concrete strength, f'_c is 20.7 Mpa (3000 psi)

Modulus of Elasticity of concrete, E_c is 21525.6 MPa (3122 ksi)
Reinforcing steel strength, f_y is 413.7 MPa (60 ksi)
Modulus of Elasticity of Reinforcement, E_s is 199948 MPa (29000 ksi)
Coefficient of Thermal Expansion for Concrete, α is 9×10^{-6} m/m per C (5×10^{-6} in/in per F)

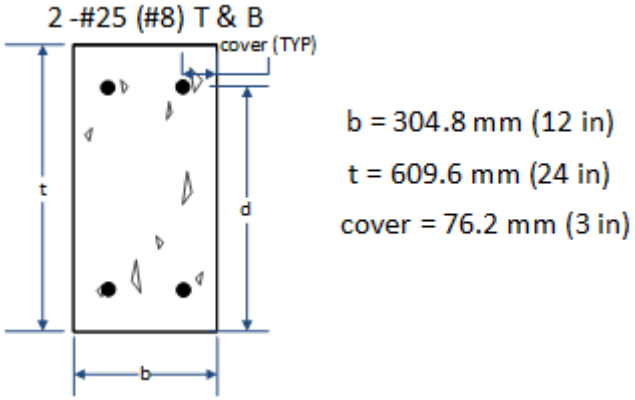

Figure 3 - Concrete Section

Section Analysis

At least three points are selected per concrete member. In other scenarios, more than 3 points may be appropriate for example for non-prismatic sections or where there are openings in the member. For this study, the points of maximum positive moment from the mechanical load case, of the maximum negative moment from the mechanical load case and of contra-flexure were chosen for the rigorous section analysis. Response of each reinforced concrete section was determined using the plane section hypothesis to compute the longitudinal strains at the chosen point for the mechanical load case, and the mechanical plus thermal load case. At each stage of loading, the strains were determined to satisfy force equilibrium and strain compatibility of the section. Once the strains at a cross section were determined, the stresses were then computed and the final moments in the sections were back calculated.

To illustrate this process, see Figure 4 for the analysis of joint B in the column for the benchmark scenario. M_B and F_{AB} are the load effects or forces from the Finite Element Model (FEM) analysis in step 1 of Figure 2. M_δ was added to the mechanical load case to account for the bulk thermal change in the horizontal beam which forces a support displacement into the columns.

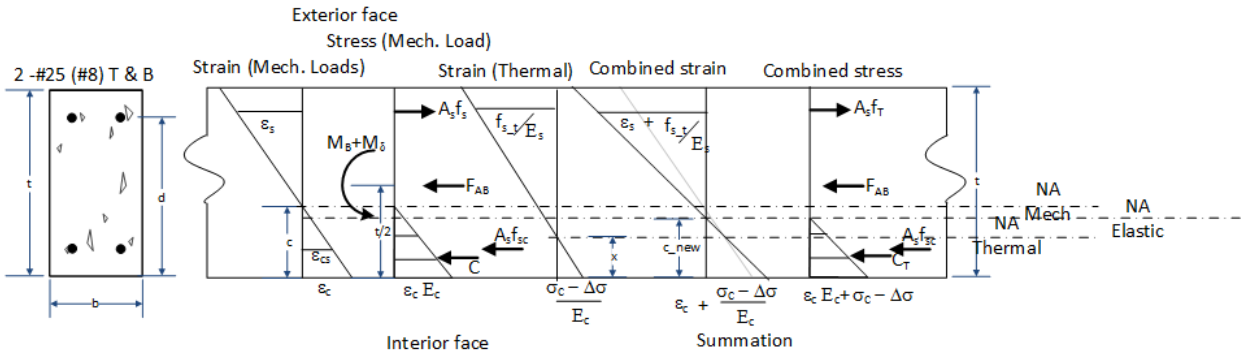

Figure 4 - Section Analysis of Cross Section at Joint B

Using force equilibrium and strain compatibility, the neutral axis (c) of the section under axial compression F_{AB} and the mechanical flexural moment M_B+M_δ was obtained to be 174.2 mm (6.9 in).

Next the strains (Figure 5) for the cracked thermal condition were determined and the neutral axis of the section (x) under thermal loading was determined to be 151.5 mm (5.96 in). Curvature for the thermal gradient is the same for the cracked and un-cracked assumptions. And since the concrete is deemed not to resisted tension, the tensile stresses are transferred to the reinforcing steel outside the compression region. This moves the thermal neutral axis down creating a loss in concrete compression. Force equilibrium is then used to determine the thermal neutral axis.

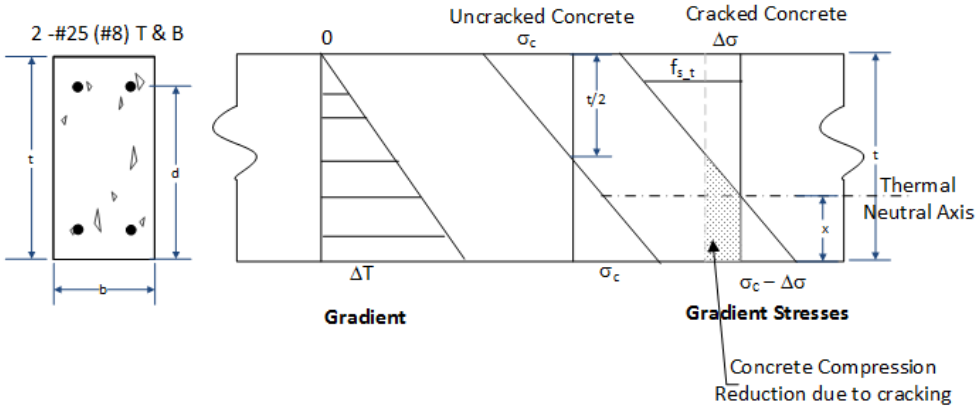

Figure 5 - Section Analysis under Thermal Gradient

The strains for the mechanical load case and the thermal gradient are added in Figure 4 to obtain the final strain state with final elastic neutral axis (c_new) determined as 169.9 mm (6.7 in). The final moment at joint B in the column is then back computed to be 150.8 kN-m (111.2 kip-ft). Since this is a section analysis, if the axial force in the column is different from that in the beam, the resulting section moment in the column will be different from the moment in the beam for the same joint. This is because section analysis does not satisfy global equilibrium hence the moments from the section analysis may not be used in design directly. The final output from the section analysis is the cracked moment of inertia. The is computed by transforming the reinforcement in tension, ignoring the reinforcement in compression and ignoring the concrete in tension to determine the geometric neutral axis (y) as shown in Figure 6.

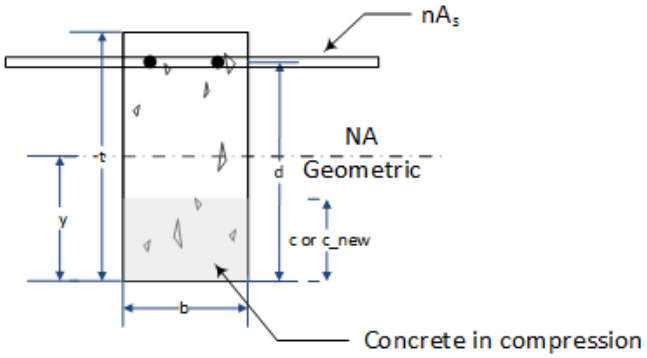

Figure 6 - Transformed Cracked Section for Mechanical Load Case and Final Load Case

A straight average of the cracked moment of inertia for the mechanical load case and the final load case which is the mechanical plus thermal load case gives a constant cracked moment of inertia that accounts for the fact that cracking is different before and after the application of the thermal gradient. For joint B, the average cracked moment of inertia (I_{B_avg}) was determined to be $0.29I_g$.

Member Analysis

Section analysis is repeated for the three points selected per concrete member. Section analysis done for the point of contra-flexure represents the point of no cracking under mechanical loads since the moment there is zero. But since thermal gradients given introduce cracking there as well, the final state may be cracked depending on how much axial compression is present in the member. For member AB, the average cracked moment of inertia at the contra-flexure (I_{CF_avg}) was $0.64I_g$.

A modified Branson (ACI 349, 2013) equation was used to provide a transition between the upper and lower bounds of I_{CF} and $I_{cracked}$ at the joints as a function of the ratio of the moment at cracking to the moment at the sections from the sectional analysis M_{cr}/M_{jt}. The moment at the joint is taken as the higher moment between the final moment including thermal loads and the moment from mechanical loads since cracks do not heal. The cracking moment is as given in ACI 318-14 with f_t used in lieu of f_r as given below. This effective moment of inertia accounts for the rate of varying cracking from the point of contra-flexure to the points of maximum negative and positive moments.

$$I_{e\_jt} = \left(\frac{M_{cr}}{M_{jt}}\right)^3 I_{CF\_avg} + \left[1 - \left(\frac{M_{cr}}{M_{jt}}\right)^3\right] I_{jt\_avg} \tag{1}$$

$$M_{jt} = max\left(M_{jt\_mech}, M_{jt\_final}\right) \tag{2}$$

$$M_{cr} = \frac{f_t I_g}{y_t} \tag{3}$$

$$f_t = 0.5\sqrt{f_c'} \quad (6\sqrt{f_c'}\ psi) \tag{4}$$

I_g is the gross moment of inertia for the cross section and y_t is the distance from the geometric neutral axis to the extreme concrete fibers in tension. The weighted average of the effective moments of inertia at the peak moments is used as the final design effective cracked moment of inertia for thermal analysis. For example for member AB the effective cracked moment of inertia was computed to be $0.32I_g$ from equation 5. L is length of the beam from a point on the beam to the next, i.e. L_{CF_B} is the length from the point of contra-flexure to joint B.

$$I_{e\_AB} = \frac{I_{e\_B}\left(L_{CF\_B}\right) + I_{e\_A}\left(L_{CF\_A}\right)}{L_{A\_B}} \tag{5}$$

PARAMETRIC CASE STUDIES

Six models studies were investigated using the methodology described in the proceeding section. First was the example problem given in chapter 3 of ACI 349.1R. This was used to benchmark the methodology. Then the axial compression in the columns was raised to 474.5 kN (350 kips) to evaluate the effect of high compression to the effective cracked moment of inertia. To study the effect of high thermal gradient, the thermal gradient was more than doubled to 72.2 ℃ (162 ℉). Finally, a moderate compression in the columns at balance point and a low compression in the columns equivalent $0.1f'_cA_g$ were also studied. The effects of the resulting effective cracked moment of inertia were compared with the effects of using $0.5EI_g$ and un-cracked concrete properties for the columns and beam.

FEM Input

It is important to manipulate both the overall depth (t) and the elastic modulus of concrete E_c of the columns and beams to run the finite element models described above using the effective cracked moment of inertia for flexure. This is because flexural stiffness is changed without changing the axial and shear stiffness of the columns and beam and to facilitate use the current thermal analysis commands for most FEM software. Manipulating t, E_c and Poisson's ratio (ν) is done by solving three simultaneous equations

to obtain t_{cr} and E_{cr} and the adjusted Poisson's ratio (ν_{cr}) such that $\lambda(EI)_{un\text{-}cracked} = (EI)_{cracked}$; $(AE)_{uncracked} = (AE)_{cracked}$; and $(GA)_{un\text{-}cracked} = (GA)_{cracked}$; λ is the factor determined by the methodology in this paper, for example λ_{AB} is 0.32 as stated in preceding section for the benchmark scenario. Solving these simultaneous equations yield that

$$t_{cr} = \sqrt{\lambda\, t^2} \tag{6}$$

$$E_{cr} = \frac{E_c}{\sqrt{\lambda}} \tag{7}$$

$$\upsilon_{cr} = \upsilon \tag{8}$$

RESULTS

If the current methodology in ACI 349.1R was investigated to back compute the effective flexural stiffness inherent in the solution, the results line up well with the result from the methodology espoused in this paper as can be seen in Table 1 and Figure 7. Negative moment produces tension on the interior face. The moment diagrams in the results have been normalized by the design moment capacity so that based on the assumption made on the flexural stiffness it can be seen how close to exceeding code capacity, the engineer perceives the problem to be. For the same temperature gradient as the benchmark problem but with high compression in columns, it is interesting to note that the final moments at joints B and C changed only slightly with the stiffness of the columns more than doubling. This is because the beam stiffness remained unchanged as can be seen in Table 2 and Figure 8. The moments at the reactions, however, are more significantly affected by the increased stiffness in the columns.

Table 1: Model 1, Benchmark model

Model: **ACI 349.1R Example Problem**	Moments at Frame joints **(kN-m/kip-ft)**				
	EI Column AB		EI Beam BC		EI Column CD
	M_A	M_B	M_{Mid}	M_C	M_D
ACI 349.1R EX – Equiv. Cracked EI	-22.1/-16.3	157.1/115.9	-32.4/-23.9	112.5/83.0	34.8/25.7
Benchmark ACI 349.1R methodology	0.41EI		0.41EI		0.33EI
ACI 349.1R EX – Cracked EI shown	25.2/-18.6	146.0/107.7	-39.3/-29.0	108.3/79.9	39.0/28.8
Effective Cracked Moment of Inertia	0.32EI		0.28EI		0.38EI
ACI 349.1R EX – Cracked Using 0.5EI as Cracked Moment of Inertia	-18.7/-13.8	162.3/119.7	-24.7/-18.2	121.6/89.7	42.7/31.5
ACI 349.1R EX Un-cracked Moment of Inertia (ABAQUS)	-0.6/-0.46	188.2/138.8	1.1/0.8	147.5/108.8	60.7/44.8
ACI 349.1R EX Un-cracked Moment of Inertia (ACI 349.1)	4.6/3.4	186.3/137.4	-0.3/-0.2	145.6/107.4	65.4/48.2

Table 2: Model 2

Model: **Low Temperature with ΔT=26.7 °C (80 °F)+ High Compression with P_{col}=474.5 kN (350 kips)**	Moments at Frame joints **(kN-m/kip-ft)**				
	EI Column AB		EI Beam BC		EI Column CD
	M_A	M_B	M_{Mid}	M_C	M_D
ACI 349.1R EX – Cracked EI shown	7.7/5.7	150.9/111.3	-37.7/-27.8	107.2/79.1	72.9/53.8
Effective Cracked Moment of Inertia	0.86EI		0.28EI		0.86EI
ACI 349.1R EX Using 0.5EI as Cracked Moment of Inertia	-21.4/-15.8	163.9/120.7	-25.1/-18.5	119.9/88.4	43.8/32.3
ACI 349.1R EX Un-cracked Moment of Inertia	-3.4/-2.5	189.4/139.7	0.70/0.53	145.6/107.4	61.8/45.6

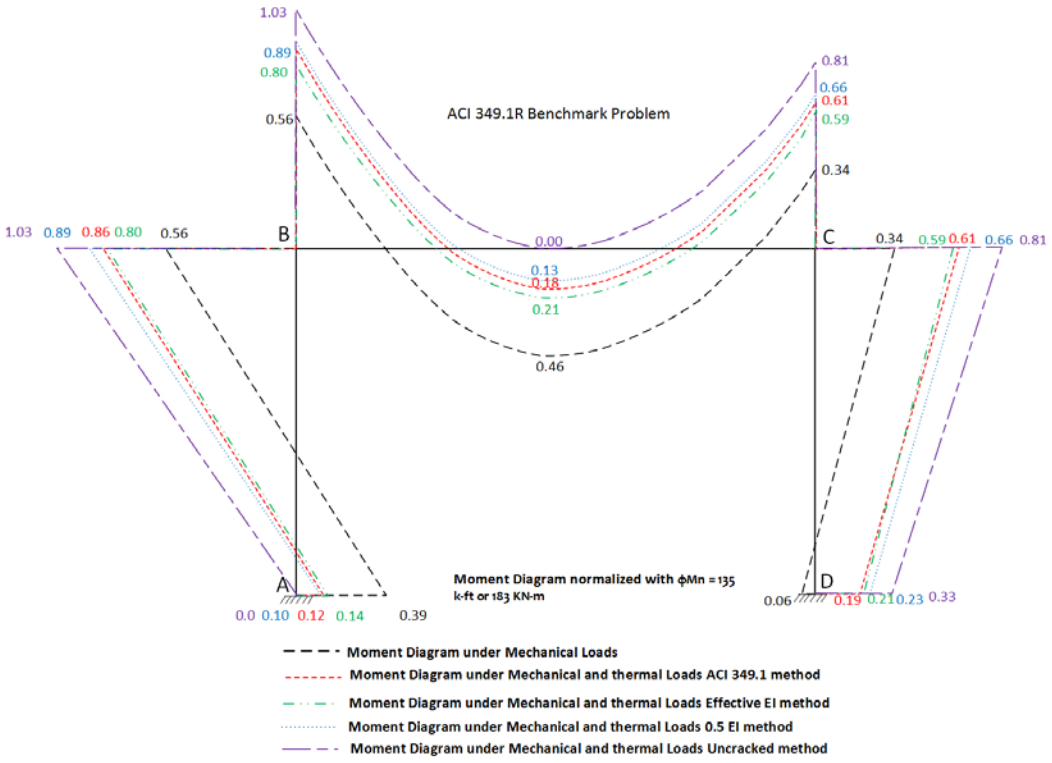

Figure 7 - Normalized Moment Diagram for Model 1

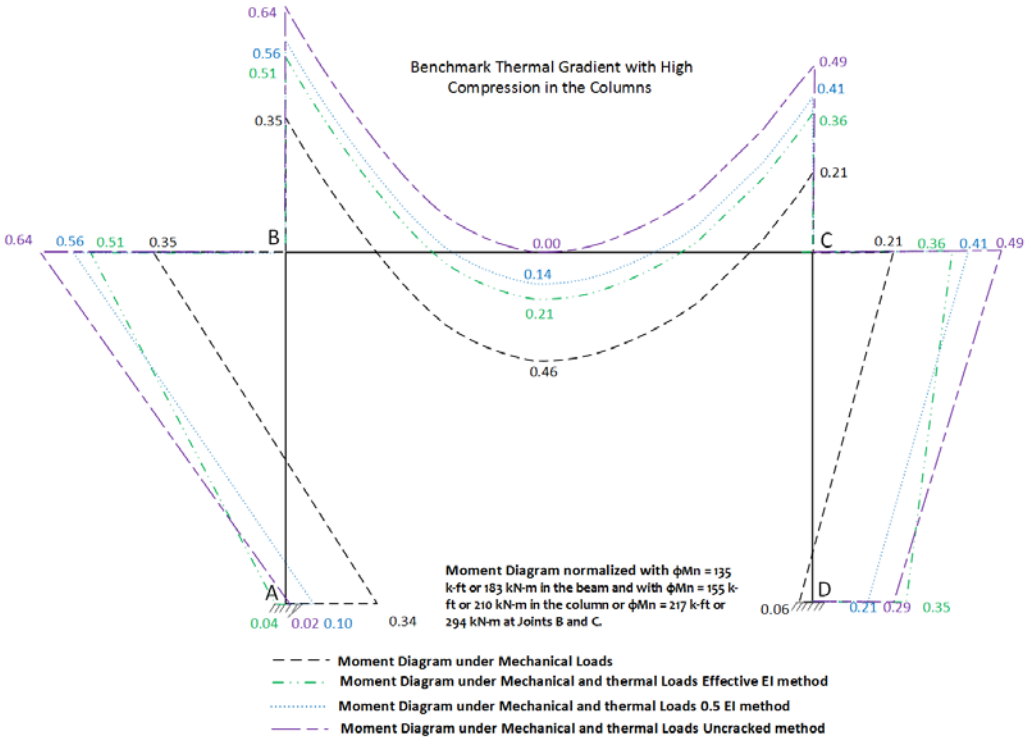

Figure 8 – Normalized Moment Diagram for Model 2

The presence of the high axial compression in the column helped the response of the columns even with the higher stiffness that resulted in higher thermal moments.

Table 3: Model 3

Model: **High Temperature with ΔT=72.2 °C (162 °F)**	Moments at Frame joints **(kN-m/kip-ft)**				
	EI Column AB		EI Beam BC		EI Column CD
	M_A	M_B	M_{Mid}	M_C	M_D
ACI 349.1R EX – Cracked EI shown	17.5/12.9	192.3/141.8	8.5/6.3	157.5/116.2	83/61.2
Effective Cracked Moment of Inertia	0.30EI		0.27EI		0.35EI
ACI 349.1R EX Using 0.5EI as Cracked Moment of Inertia	28.9/21.3	226.2/166.8	39.2/28.9	185.5/136.8	90.2/66.5
ACI 349.1R EX Un-cracked Moment of Inertia	59.7/44.0	280.7/207	93.6/69.0	240/177.0	120.9/89.2

With the thermal gradient more than doubled in Table 3, it was observed that the flexural stiffness only reduced slightly by about 3.5 to 8% so cracking only increased slightly with higher thermal gradient. But without the presence of high compression helping, it is noticed in Figure 9, that the thermal gradient caused the joint B to exceed code capacity for all stiffness scenarios. So if high compression was re-introduced the compression helping the response is once again noticed as given in Table 4 and Figure 10.

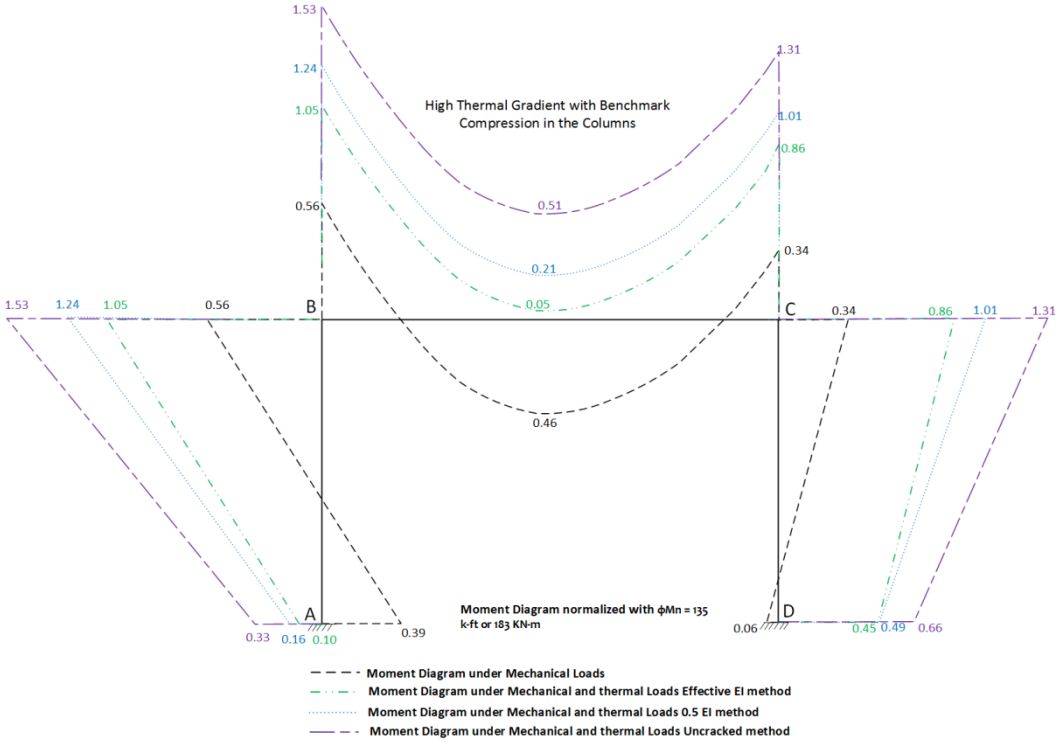

Figure 9 - Normalized Moment Diagram for Model 3

Table 4: Model 6

Model: **High Temperature with ΔT=72.2 °C (162 °F))+ High Compression with P_{col}=474.5 kN (350 kips)**	Moments at Frame joints **(kN-m/kip-ft)**				
	EI Column AB		EI Beam BC		EI Column CD
	M_A	M_B	M_{Mid}	M_C	M_D
ACI 349.1R EX – Cracked EI shown	73.5/54.2	200.9/148.2	11.1/8.2	155.1/114.4	136.9/101.0
Effective Cracked Moment of Inertia	0.80EI		0.27EI		0.74EI
ACI 349.1R EX Using 0.5EI as Cracked Moment of Inertia	26.0/19.2	227.4/167.7	38.8/28.6	183.6/135.4	91.2/67.3
ACI 349.1R EX Un-cracked Moment of Inertia	56.8/41.9	281.9/207.9	93.1/68.7	238.1/175.6	122.0/90.0

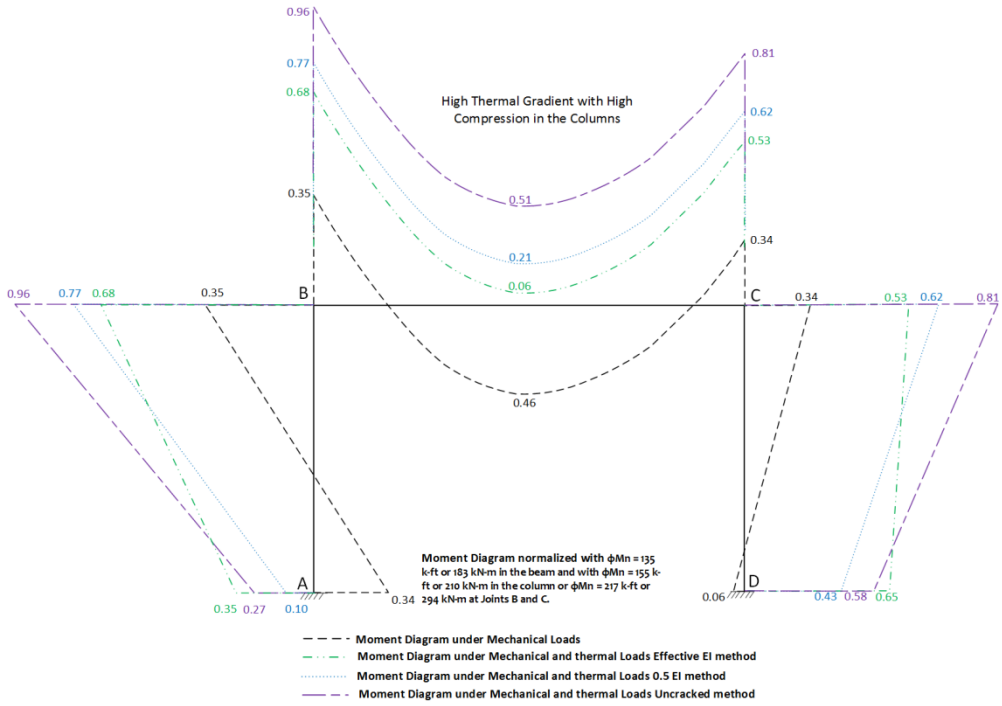

Figure 10 - Normalized Moment Diagram for Model 6

Models 4 and 5 with compression in the columns equal to $\phi P_n = 0.1f'_cA_g$. and ϕP_b respectively yielded effective cracked stiffness of 0.33EI and 0.61EI for member AB and 0.42EI and 0.66EI for member CD respectively. The cracked stiffness of the beam remained constant at 0.27Ei for both models.

CONCLUSION

From the models investigated it can be seen that under no circumstance was it advantageous to use un-cracked concrete properties for thermal gradient analysis when the thermal moment in un-cracked concrete is greater than the cracking moment. That threshold for this frame's cross section and reinforcing was approximately ΔT=10°C (50°F). So for thermal gradient greater than this threshold cracked properties of concrete must be used. ACI Committee 349 recognizes that un-cracked lengths exist in a member near the regions of contra-flexure, so this method accounts for variability in cracking along the length of the member by using the effective moment of inertia determined by a modified Branson's formula.

The design of the frame used in this paper is controlled by the design of joints B and C where the thermal moments are additive to the moments from the mechanical load case. Thermal loads are added after the mechanical loads have been realized. For most accidental thermal case, this scenario bears out. The structure sees the thermal load case only after it has seen the design mechanical load case. In operating thermal load case, it could be argued that the structure does not see the worst case mechanical load case before the thermal load case is applied. This methodology could be adapted to the operating load case as well. The only recommended modification would be to use two mechanical load cases, one that is more probable to occur before the thermal load case to conduct the section analysis and obtain the effective cracked conditions and the other mechanical load case to add to the thermal case for the final moments. Figure 11 shows the P-M diagrams for joints B and C but with the final axial and moment load effects plotted in terms of the cracked stiffness used to compute them. A pattern is seen to emerge from the data which informs the conclusion shown in Table 5.

In the introduction of this paper, we mentioned that ACI committee 349 is seeking to go to cracked stiffness for seismic given in ASCE 43 for use in thermal load analysis. In other words, use the cracking

that occurs under mechanical loads to determine the thermal moments. This paper finds that approach an improvement but still conservative. This is because this approach ignores further cracking that occurs under thermal loads. This methodology uses the average of the before thermal and the after thermal cracking to determine the thermal moments. This is a more realistic approach. It was, however, recognized during the course of the parametric study that the thermal moments were not very sensitive to the exact cracked moment of inertia but more to the relative stiffness between the cracked concrete members. For example model 3 with high thermal gradient and the benchmark compression in member CD yielded a cracked flexural stiffness of 0.35EI but a final moment at joint C of 157.5 kN-m (116.2 kip-ft) and Model 4 with high thermal gradient and low compression of $0.1f'_cA_g$ yielded a cracked flexural stiffness of 0.42EI and a final moment of 157.4 kN-m (116.1 kip-ft). This observation helps the conclusion reached in this paper given in Table 5.

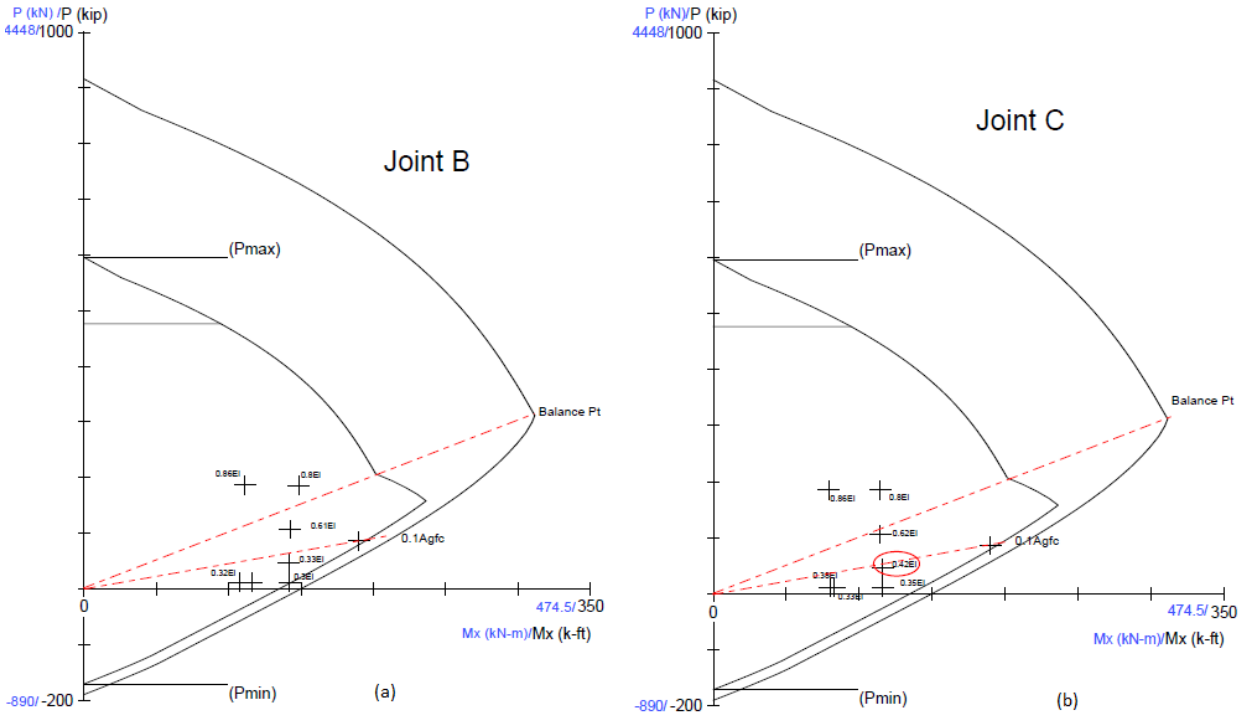

Figure 11 - P-M Diagram for Joints B and C

Table 5: Effective Stiffness Values

Component	Flexural Rigidity ASCE 43	Flexural Rigidity ACI 349.1R	Paper Recommendation	Comment
Beams – $P<0.1f'_cA_g$	$0.5E_cI_g$	$0.5E_cI_g$	$0.3E_cI_g$	Applicable when peak member moments from mechanical load case are greater than M_{cr} and thermal gradients greater than $\Delta T=10°C$ (50°F)
Beams $-0.1f'_cA_g \leq P<\phi P_b$	$0.5E_cI_g$	$0.5E_cI_g$	$0.5E_cI_g$	
Columns – $P<\phi P_b$	$0.7E_cI_g$	$0.5E_cI_g$	$0.5E_cI_g$	
Columns–$P>\phi P_b$	$0.7E_cI_g$	$0.5E_cI_g$	$0.8E_cI_g$	

Note that this paper recommends the use of 0.8EI for columns instead of the 0.7EI given in ASCE 43. This recommendation is neither less conservative nor more conservative. The results will be comparable and the error introduced by using 0.7EI negligible. This is because, though 0.8EI will result in slightly higher thermal moments, it was observed that compression also helped the column's response

hence reducing the demand to capacity ratios as can be seen from the shape of the P-M curves and from comparing Figures 9 and 10.

Finally, ACI 349 recommends that thermal load effects shall not be used to reduce mechanical load effects. This paper concurs with that requirement. As can be seen in Figures 7 through 9 that the effects of the stiffness values assumed was significant on joints A and D where thermal effects were contrary to the mechanical load effects. In design, ACI 349 requires that the envelope of moments (i.e. mechanical loads and final loads) at joints A and D be accounted for in design. One should do this as a matter of good practice because of the simplifications in the rigorous section analysis and because most designs do not account for thermal relaxation. Thermal relaxation will in time undo some of the stress relief observed for joints A and D.

These values in Table 5 have not been studied for walls or diaphragms and it is advised for future work to conduct this investigation. It is the hope that the values given in Table 5 may extend to walls and diaphragms as well.

ACKNOWLEDGEMENTS

This paper is part of an on-going effort by ACI 349 to revise ACI 349.1R. The authors would like to express gratitude for the support of the following: Mr. Jim Rugg, Dr. Shawn Carey, Mr. Jay Amin and Mr. Roy Rothermel. Dr Adediran is the current Chair of ACI 349 and Mr Ghosal is a current vice chair of ACI 349.

REFERENCES

ACI349.1R, (2007). “Reinforced Concrete Design for Thermal Effects on Nuclear Power Plant Structures,” *American Concrete Institute Committee 349*, Michigan, USA.

ACI318M, (2014). “Building Code Requirements for Structural Concrete and Commentary (Metric),” *American Concrete Institute Committee 318*, Michigan, USA.

ACI349, (2006). “Code Requirements for Nuclear Safety-Related Concrete Structures and Commentary (Metric),” *American Concrete Institute Committee 349*, Michigan, USA.

ASCE/SEI 43, (2005). “Seismic Design Criteria for Structures, Systems and Components in Nuclear Facilities,” American Society of Civil Engineers, Virginia, USA.